

Title: Impact of Bioresorbable Scaffold Design Characteristics on Local Hemodynamic Forces - an ex vivo Assessment with Computational Fluid Dynamics Simulations.

Authors: Imane Tarrahi, MSc; Monika Colombo, MSc; Eline M.J. Hartman, M.D; Maria Natalia Tovar Forero, M.D; Ryo Torii, PhD; Claudio Chiastra, PhD; Joost Daemen, M.D, PhD; Frank J.H. Gijsen, PhD

DOI: 10.4244/EIJ-D-19-00657

Citation: Tarrahi I, Colombo M, Hartman EMJ, Tovar Forero MN, Torii R, Chiastra C, Daemen J, Gijsen FJH. Impact of Bioresorbable Scaffold Design Characteristics on Local Hemodynamic Forces - an ex vivo Assessment with Computational Fluid Dynamics Simulations. *EuroIntervention* 2020; Jaa-717 2020, doi: 10.4244/EIJ-D-19-00657

Manuscript submission date: 16 July 2019

Revisions received: 02 December 2019

Accepted date: 15 January 2020

Online publication date: 21 January 2020

Disclaimer: This is a PDF file of a "Just accepted article". This PDF has been published online early without copy editing/typesetting as a service to the Journal's readership (having early access to this data). Copy editing/typesetting will commence shortly. Unforeseen errors may arise during the proofing process and as such Europa Digital & Publishing exercise their legal rights concerning these potential circumstances.

Impact of Bioresorbable Scaffold Design Characteristics on Local Hemodynamic Forces - an ex vivo Assessment with Computational Fluid Dynamics Simulations

Imane Tarrahi¹, MSc; Monika Colombo², MSc; Eline M.J. Hartman¹, MD; Maria Natalia Tovar Forero³, MD; Ryo Torii⁴, PhD; Claudio Chiastra⁵, PhD; Joost Daemen³, MD, PhD; Frank J.H. Gijsen¹, PhD

¹ Department of Biomedical Engineering, Erasmus MC, Rotterdam, The Netherlands

² LaBS, Dept. of Chemistry, Materials and Chemical Engineering “Giulio Natta”, Politecnico di Milano, Milan, Italy

³ Department of Cardiology, Erasmus MC, Rotterdam, The Netherlands

⁴ Department of Mechanical Engineering, University College London, London, United Kingdom

⁵ PoliToBIOMed Lab, Dept. of Mechanical and Aerospace Engineering, Politecnico di Torino, Turin, Italy

Short running title:

The Impact of Various Bioresorbable Scaffold Designs on Hemodynamics

Corresponding author:

Frank J.H. Gijsen, PhD

Postal address: 1738, 3000 DR Rotterdam, the Netherlands

E-mail address: f.gijsen@erasmusmc.nl

Conflict of interest:

The authors have no conflict of interest to declare.

Portrait:



Disclaimer : As a public service to our readership, this article -- peer reviewed by the Editors of EuroIntervention - has been published immediately upon acceptance as it was received. The content of this article is the sole responsibility of the authors, and not that of the journal

Abstract

Aim:

Bioresorbable scaffold (BRS) regions exposed to flow-recirculation, low time-averaged wall shear stress (TAWSS) and high oscillatory shear index (OSI), develop increased neo-intima tissue. We investigated hemodynamic features in 4 different BRSs.

Methods and results:

Fantom (strut height (SH) = $125\mu\text{m}$), Fantom Encore (SH = $98\mu\text{m}$), Absorb (SH = $157\mu\text{m}$) and Magmaris (SH = $150\mu\text{m}$) BRSs were deployed in phantom tubes and imaged with microCT. Both 2D and 3D geometrical scaffold models were reconstructed. Computational fluid dynamics (CFD) was performed to compute TAWSS and OSI.

Thicker struts had larger recirculation zones and lower TAWSS in 2D. Absorb had the largest recirculation zone and lowest TAWSS ($240\mu\text{m}$ and -0.18 Pa), followed by Magmaris ($170\mu\text{m}$ and -0.15 Pa), Fantom ($140\mu\text{m}$ and -0.14 Pa) and Fantom Encore ($100\mu\text{m}$ and -0.13 Pa). Besides strut size, stent design played a dominant role in 3D. The highest percentage area adverse TAWSS ($<0.5\text{ Pa}$) and OSI (>0.2) were found for Fantom (56% and 30%) and Absorb (53% and 33%), followed by Fantom Encore (30% and 25%) and Magmaris (25% and 20%). Magmaris had the smallest areas due to a small footprint and rounded struts.

Conclusion:

Due to stent design both Fantom Encore and Magmaris showed smaller TAWSS and OSI than Fantom and Absorb. This study quantifies which scaffold features are most important to reduce long-term restenosis.

Condensed abstract:

Low and oscillating wall shear stress (WSS) in coronary arteries can lead to neo-intimal growth of vascular tissue. Stent and scaffold design can largely influence the WSS patterns in arteries. This study compared hemodynamic features in 4 scaffolds: Fantom Encore,

Disclaimer : As a public service to our readership, this article -- peer reviewed by the Editors of EuroIntervention - has been published immediately upon acceptance as it was received. The content of this article is the sole responsibility of the authors, and not that of the journal

Fantom, Magmaris and Absorb. The results suggest that both Fantom Encore and Magmaris create the smallest areas of low and oscillating WSS, due to smaller struts, good strut and connector alignment and large inter-strut distance.

Keywords:

In-stent restenosis; Bioresorbable scaffolds; Pre-clinical research

Abbreviations:

BRS	bioresorbable vascular scaffold
TAWSS	time averaged wall shear stress
OSI	oscillatory shear index
CFD	computational fluid dynamics
DES	drug eluting stent

Introduction

The efficacy of metallic stents and bioresorbable scaffolds (BRS) to treat coronary artery stenosis is related to the hemodynamic environment [1]. The struts of these devices disturb the local flow field and induce regions with low and oscillating wall shear stress[2–5]. These flow disturbances are related to various pathological processes. Low wall shear stress is associated with increased neo-intimal growth [4,6–9], delayed re-endothelialisation [1,10] and an increased risk of stent thrombosis [1,5,11] .

The magnitude of blood flow disruption is influenced by scaffold design. It was shown that strut height and shape influence the size of flow recirculation zones [12,13]. Furthermore, larger strut spacing restores the blood flow profile between struts [12,13]. Alignment of the general stent lay-out to blood flow also determines the region exposed to low and oscillating wall shear stress [13,14].

BRS are designed to dissolve over time, which has the potential benefit of restoring vasomotion, leave the option open for future bypass surgery with graft anastomoses at the scaffolded segments, and reduce late stent related adverse events [15,16]. Typically, a BRS consists of bioresorbable polymers or metals that are inherently weaker than conventional non-resorbable metallic stents. Therefore, more material is needed to provide adequate support to the artery. As a result, BRS have relatively thick struts with more pronounced hemodynamic impact as compared to current generation thin strut metallic drug-eluting stents (DES)[17].

In this context, the aim of this work is to compare the impact of 4 different BRS designs on local hemodynamics using computational fluid dynamics (CFD). Three devices are characterized by a rectangular strut profile, namely Fantom Sirolimus-Eluting Bioresorbable Scaffold (REVA Medical, San Diego, CA, USA), Fantom Encore Tyrocore Bioresorbable Scaffold (REVA Medical, San Diego, CA, USA) and Absorb everolimus-eluting Bioresorbable Vascular Scaffold GT-1 (Abbott Vascular, Santa Clara, CA, USA). One device is characterized by more rounded strut edges, namely Magmaris Resorbable Magnesium Scaffold (Biotronik, Berlin, Germany).

Methods

To investigate the effect of the individual scaffold designs, we used two different approaches. Firstly, a two dimensional (2D) analysis was performed to elucidate the effect of strut height and shape. Secondly, a three dimensional (3D) analysis was carried out to investigate the combined effects of strut height, strut shape and scaffold layout.

Scaffold reconstruction

The main characteristics of the 4 studied scaffolds are presented in Table 1. We compared

Disclaimer : As a public service to our readership, this article -- peer reviewed by the Editors of EuroIntervention - has been published immediately upon acceptance as it was received. The content of this article is the sole responsibility of the authors, and not that of the journal

the Fantom (REVA Medical) with a strut thickness of 125 μm , Fantom Encore (REVA Medical) with a strut thickness of 98 μm , Absorb (Abbott Vascular) with a strut thickness of 157 μm and the Magmaris (Biotronik) with a strut thickness of 150 μm .

Firstly, the scaffold struts were reconstructed in 2D (Figure 1A). The strut height, width and shape were based on data provided by the manufacturer. The inter-strut distance was repeatedly measured and the average inter-strut distance was determined for each scaffold. The distance between struts for all 2D models was the average inter-strut distance of all real scaffolds, namely 975 μm . The complete 2D geometry consisted of 5 consecutive struts placed on top and bottom of a flat cylinder. In addition, in order to study the effects of changes in strut height, strut width and inter-strut distance, we created hypothetical 2D strut models with a 20% decrease in height, in width and in inter-strut distance. To study the effects of the rounded strut edges in Magmaris, a model with rectangular struts of the same size was made.

Secondly, the scaffolds were reconstructed in 3D (Figure 1B). Each of the scaffolds was deployed inside a plastic phantom tube, according to the guidelines of the scaffold suppliers. After expansion, the in vitro models were imaged with microCT with an isotropic resolution of 20 μm (Quantum FX, PerkinElmer, Waltham, USA). The centrelines of the scaffolds were extracted from the microCT data using Mimics (Materialise, Belgium), resulting in the skeletonized scaffolds. Subsequently, the reconstructed 2D struts were placed over the 3D skeletons using a previously developed semiautomatic procedure in Rhinoceros (v.5, Robert McNeel & Associates, Seattle, WA, USA) [18]. A surface was lofted over each of the 2D strut shapes resulting in the complete surface of the scaffolds [18]. Finally, the geometries of each of the scaffolds and the surrounding tubes were merged in ICEM CFD (v.17.1, ANSYS Inc., Canonsburg, PA, USA).

Disclaimer : As a public service to our readership, this article -- peer reviewed by the Editors of EuroIntervention - has been published immediately upon acceptance as it was received. The content of this article is the sole responsibility of the authors, and not that of the journal

Geometry Discretization

After geometry reconstruction, the surfaces were discretized into elements in ICEM CFD (v.17.1, ANSYS Inc., Canonsburg, PA, USA). A mesh independence study was performed in order to optimize the computational efficiency without decreasing the solution accuracy. The resulting typical element sizes were 0.015 mm and 0.1 mm for the scaffolded region and the non-stented regions, respectively. The final discretized models were composed of around 5 million elements, which is comparable to previous studies [19].

Computational Fluid Dynamics

Transient CFD simulations were performed with a generic left anterior descending coronary artery inlet flow profile mimicking pulsatile physiological conditions [20] and zero reference pressure at the outlet using Fluent (v.17.1, ANSYS Inc., Canonsburg, PA, USA). The mean flow rate was scaled to a steady flow rate with maximum velocity of 0.15 m/s. In addition, the TAWSS at the inlet was kept the same for all scaffolds by scaling the inflow accordingly. The vessel wall was considered rigid with no-slip condition. Blood inside the reconstructed stented geometrical model was assumed to be non-Newtonian, behaving according to the Carreau model [21], with mass density of 1060 kg/m³. One and a half heart cycles were simulated, using 150 time steps. The first half of the simulated cardiac cycle was disregarded in order to eliminate start-up effects [22]. Both the inlets and outlets of the 3D geometries were extended by 3 times the diameter to make sure that the simulated flow was fully developed before entering the stented region and to reduce the effect of outflow boundary conditions [23].

Hemodynamic quantities of interest

The TAWSS and OSI were derived from the computed time dependent velocity field. The TAWSS is the mean wall shear stress over 1 heart cycle. TAWSS values lower than 0.5 Pa have been associated with increased neo-intimal formation [24]. Therefore, adverse TAWSS

was defined as <0.5 Pa. In addition, the OSI was extracted from the performed simulations. If blood flow is recirculated, the wall shear stress also changes direction. OSI captures the amount of directional change of wall shear stress in 1 heart cycle. Ranging from 0 to 0.5 (unit less), higher OSI values have been associated with increased neo-intimal formation [25,26]. In this paper, adverse OSI was defined as >0.2 .

Data analysis

The CFD results of the 3D phantom wall in scaffolded regions were post-processed in CFD-Post (v.17.1, ANSYS Inc., Canonsburg, PA, USA) and analysed with MATLAB (R2018a, Mathworks, Natick, MA, USA). The vessel wall was divided into segments of 4 degrees in circumference and 50 micron in length. These segments were used for generating a 2D contour map of the TAWSS and OSI. Only the regions between struts were included. Histograms were made in order to analyse the distributions in terms of their skewness, kurtosis and standard deviation. Kolmogorov Smirnov test was used to test the distributions for normality ($p < 0.001$). Kruskal-Wallis test was used to test similarity in the distributions of the scaffolds. The percentage lumen area with low TAWSS and high OSI was determined in scaffolded regions for all scaffolds.

Results:

2D simulations

Figure 2 illustrates the blood flow patterns in 2D simulations. The velocity streamlines and vectors between 2 adjacent struts are displayed for each scaffold. The velocity vectors distal of the struts point in opposite direction of the blood flow, indicating the presence of a distal recirculation zone. After the distal recirculation zone, the streamlines run parallel to the wall again, which indicates the restoration of blood flow. This zone is labelled as the recovery zone. Proximal to the next strut another recirculation of blood flow can be observed, which is

defined as the proximal recirculation zone. The proximal recirculation zone is smaller than

Disclaimer : As a public service to our readership, this article -- peer reviewed by the Editors of EuroIntervention - has been published immediately upon acceptance as it was received. The content of this article is the sole responsibility of the authors, and not that of the journal

the distal recirculation zone. The sizes of the distal recirculation zone and proximal recirculation zone increases with increasing strut height, whilst the size of the recovery zone decreases with strut height.

In Figure 3 the TAWSS between struts is shown. The distal and proximal recirculation zones have zero and negative TAWSS, whilst the recovery zone has positive TAWSS values.

Fantom Encore has a minimal TAWSS of -0.12 Pa in the distal recirculation zone, with a recirculation zone length of 0.10 mm, which is equal to 17% of the distance between struts.

In the recovery zone, the TAWSS peaks at 0.45 Pa. The proximal recirculation zone is smaller than the distal recirculation zone (0.07 mm, 12%) with a higher minimal TAWSS value (-0.07 Pa). The sizes of the recirculation zones increase with increasing strut height, whilst the minimal, maximal TAWSS and size of the recovery zone decreases with strut height.

A positive trend is shown between strut thickness and distal recirculation zone in Figure 4. A negative trend is shown between peak TAWSS and strut thickness and between minimum TAWSS and strut thickness. Compared to rectangular strut edges, rounded strut edges show relatively smaller recirculation zones, higher peak TAWSS in the recovery zone and higher minimum TAWSS in the recirculation zones.

In Table 2 the effects of changes of the scaffold features are quantified in 2D simulations.

Strut thickness changes the size of the distal recirculation zone, the minimum and maximum TAWSS values the most. Inter-strut distance does not change the minimum TAWSS and the recirculation zone as much; however, it has a larger effect on the maximum TAWSS value compared to strut thickness. Rounding the strut edges has a smaller effect, while strut width does not affect any of the analysed quantities considerably. The maximum OSI values seem not considerably affected by any factor.

3D simulations

Figures 5A and 5B show the distribution of the TAWSS and OSI for each scaffold in 3D, in which the effect of different scaffold design on TAWSS and OSI is demonstrated. Low TAWSS and high OSI are visible near the struts. Elevated TAWSS and lower OSI values are visible between struts, near the cell centre. This is further illustrated in the unwrapped TAWSS distribution of Fantom Encore in Figure 5C. The recirculation zones and recovery zones are visible near struts, comparable to the features observed in 2D. In addition, the zoomed single cell highlights the variations of TAWSS within a cell, presenting the combined effect of the scaffold layout and deployment.

Figure 6 shows the distribution of TAWSS and OSI per scaffold. The percentage area with low TAWSS (< 0.5 Pa) and high OSI (> 0.2) is also denoted. Both TAWSS and OSI distributions of the scaffolds were significantly different ($p < 0.001$), see Table 3. The percentage area with low TAWSS for Fantom is 56%, for Fantom Encore it is approximately half of the percentage area. Absorb has slightly less amount of low TAWSS (53%) and Magmaris has the least amount of low TAWSS (26%). The percentage area with high OSI for Fantom is 31%, whilst for Fantom Encore it is 24%. Absorb has the highest amount of high OSI (33%), whilst Magmaris has the least amount of high OSI (20%).

Discussion:

In this study the hemodynamic behaviour of 4 BRSs was investigated by means of computational techniques. The effects of scaffold design, lay-out and strut sizes on TAWSS and OSI were analysed. These metrics provide a tool for assessing the mid- to long-term safety and efficacy of scaffolds. In 2D, the strut height proved to be the main determinant of the computed flow features. In 3D, both strut design and the overall scaffold lay-out influenced the distribution of TAWSS and OSI.

Disclaimer : As a public service to our readership, this article -- peer reviewed by the Editors of EuroIntervention - has been published immediately upon acceptance as it was received. The content of this article is the sole responsibility of the authors, and not that of the journal

Firstly, the scaffolds were compared in a 2D simulation, in which the impact of strut height, width, shape and the inter-strut distance on the distal recirculation zone, the minimum and maximum TAWSS values was illustrated. The quantitative analysis showed that strut height is nearly linearly related to the hemodynamic quantities analysed for struts with a rectangular shape, confirming previous studies [12,27]. Rounding of strut edges in case of Magmaris reduces the size of recirculation zones by 7%, the minimum TAWSS by 7% and increases the peak TAWSS by 4%, which illustrates the positive effect of rounding of strut shape on the hemodynamic microenvironment, which corroborates previous findings [17].

Interestingly, a decrease in inter-strut distance does not seem to have a major effect on the recirculation zone size and minimum TAWSS, however, the maximum TAWSS value in the recovery zone is considerably reduced. In essence, depending on the threshold of low TAWSS, there are fewer areas of normal TAWSS on the arterial wall. This illustrates the interplay between strut height and inter-strut distance. The OSI values seem not be considerably affected by any of the factors, the reason remains to be investigated.

Secondly, the scaffolds were compared to each other in 3D simulations. The flow features observed in 2D simulations were also present in 3D, including the distal recirculation zone, recovery zone and proximal recirculation zone. However, the effect of strut height was not as dominant. In the 2D simulations, the decrease of strut height from Fantom (125 μm) to Fantom Encore (98 μm) is 27 μm (22%), which caused the recirculation zones to decrease with 37%. Going from Fantom to Fantom Encore in 3D led to a 17% reduction of low TAWSS area, which is less of a reduction compared to the 2D case (17% vs. 37%, respectively).

Scaffolds contain connectors and v-shaped rings, which cannot be modelled in 2D. These rings and connectors add to the disturbance of the 3D flow profiles, causing the reduction of low TAWSS area to be less in 3D.

In addition, the cell lay-out in 3D considerably influences the sizes of recovery zones [14]. An open cell design results in larger recovery zones, and thus smaller areas with low TAWSS and high OSI [22]. This explains the comparable areas of low TAWSS and high OSI of Fantom and Absorb, despite Absorb having thicker struts. Magmaris also has thicker struts than Fantom; however, the areas of low TAWSS and high OSI were considerably smaller. In fact, Magmaris had the least amount of adverse TAWSS and OSI due to both the rounded strut edges and the scaffold design. As previous studies have shown, smaller areas of low TAWSS values at baseline after scaffold implantation have been associated with an increase in lumen area long-term [28]. Therefore, one of the selection criteria of scaffolds should be the hemodynamic performance at baseline. Thin struts are often considered as the main predictor of good hemodynamic performance, however, the results of this study show that open cell scaffolds might be just as effective in reducing regions with low TAWSS and high OSI. The role of designers is to find a balance between the minimum strut height needed for sufficient radial force and the maximum strut height for minimal low TAWSS and high OSI areas.

Limitations:

The 3D models were based on the geometry obtained after deployment of BRS in straight plastic tubes. This has two important implications. Firstly, the 3D curvature of the coronary arteries was not included. The 3D curvature will induce secondary flows and, therefore, asymmetrical velocity profiles will develop with higher velocities at the outer curve, and lower velocities at the inner curve [29]. However, since this effect depends on shape of the artery and not on scaffold design, 3D curvature is expected to have a comparable effect for all scaffolds. Secondly, the plastic tube was not rigid but not as compliant as the vessel wall tissue. This prevents embedding of struts, a feature observed in coronary arteries [30]. This will influence strut protrusion, effectively changing strut height. This will affect the

hemodynamic environment in vivo [17]. How and whether stent and strut design changes strut protrusion in vivo is also determined by the properties of the diseased vessel wall and remains to be investigated.

Conclusion:

In this study, scaffolds with relatively thicker struts turned out to have smaller areas of low TAWSS. This was due to a larger inter-strut distance and due to rounding of the strut edges, presenting the added significance of both scaffold design features. Out of the 4 investigated BRS, Magmaris and Fantom Encore perform best in terms of local hemodynamics. This study shows the significance of strut shape and scaffold layout, suggesting that scaffolds with thicker struts can perform better than scaffolds with thinner struts if the shape and layout are chosen wisely.

Impact on daily practice:

This study shows the extent of the effect each of the scaffold design features on low TAWSS and high OSI. Based on these results, an open scaffold design proved to be one of the major determinants of favourable blood flow profile and should be considered in both the selection of a scaffold as well as scaffold designing. Choosing a scaffold that induces higher endothelial TAWSS and lower OSI at baseline after deployment increases lumen area long-term.

Funding:

This project has received funding from the European Union's Horizon 2020 research and innovation programme under grant agreement No 777119.

References:

1. Heiden K Van Der, Gijsen FJH, Narracott A, Hsiao S, Halliday I, Gunn J, Wentzel JJ, Evans PC. The effects of stenting on shear stress : relevance to endothelial injury and repair. *Cardiovasc Res*. 2013;99:269–75.
2. Gijsen FJH, Oortman RM, Wentzel JJ, Schuurbiers JCH, Tanabe K, Degertekin M, Ligthart JM, Thury A, De Feyter PJ, Serruys PW, Slager CJ. Usefulness of Shear Stress Pattern in Predicting Neointima Distribution in Sirolimus-Eluting Stents in Coronary Arteries. *Am J Cardiol*. 2003;92:1325–8.
3. Kolandaivelu K, Swaminathan R, Gibson W, Kolachalama V, Nguyen-Ehrenreich K-L, Giddings VL, Coleman L, Wong GK, Edelman ER. Stent thrombogenicity early in high risk interventional settings driven by stent design and deployment, and protected by polymer-drug coatings. *Circulation*. 2011;123:1400–9.
4. Ladisa JF, Olson LE, Molthen RC, Hettrick DA, Pratt PF, Hardel MD, Kersten JR, Warltier DC, Pagel PS. Alterations in wall shear stress predict sites of neointimal hyperplasia after stent implantation in rabbit iliac arteries. *Am J Physiol Hear Circ Physiol*. 2005;288:2465–75.
5. Ng J, Bourantas C V, Torii R, Ang HY, Tenekecioglu E, Serruys PW, Foin N. Local hemodynamic forces after stenting. Implications on Restenosis and Thrombosis. *Arter Thromb Vasc Biol*. 2017;37:2231–42.
6. Wentzel JJ, Krams R, Schuurbiers JCH, Oomen JA, Kloet J, Van Der Giessen WJ, Serruys PW, Slager CJ. Relationship Between Neointimal Thickness and Shear Stress After Wallstent Implantation in Human Coronary Arteries. *Circulation*. 2001;103:1740–5.

7. Papafaklis MI, Bourantas C V, Theodorakis PE, Katsouras CS, Naka KK, Fotiadis DI, Michalis LK. The Effect of Shear Stress on Neointimal Response Following Sirolimus- and Paclitaxel-Eluting Stent Implantation Compared With Bare-Metal Stents in Humans. *JACC Cardiovasc Interv.* 2010;3:1181–9.
8. Bourantas C V, Räber L, Zaugg S, Sakellarios A, Taniwaki M, Heg D, Moschovitis A, Radu M, Papafaklis MI, Kalatzis F, Naka KK, Fotiadis DI, Michalis LK, Serruys PW, Garcia Garcia HM, Windecker S. Impact of local endothelial shear stress on neointima and plaque following stent implantation in patients with ST-elevation myocardial infarction : A subgroup-analysis of the COMFORTABLE AMI – IBIS 4 trial. *Int J Cardiol.* 2015;186:178–85.
9. Stone PH, Coskun AU, Kinlay S, Popma JJ, Sonka M, Wahle A, Yeghiazarians Y, Maynard C, Kuntz RE, Feldman CL. Regions of low endothelial shear stress are the sites where coronary plaque progresses and vascular remodelling occurs in humans: an in vivo serial study. *Eur Heart J.* 2007;28:705–10.
10. Tenekecioglu E, Poon EKW, Collet C, Thondapu V, Torii R, Bourantas C V, Zeng Y, Onuma Y, Ooi ASH, Serruys PW, Barlis P. The Nidus for Possible Thrombus Formation. *JACC Cardiovasc Interv.* 2016;9:2167–8.
11. Palmerini T, Benedetto U, Biondi-Zoccai G, Riva DD, Bacchi-reggiani L, Smits PC, Vlachojannis GJ, Jensen LO, Christiansen EH, Berencsi K, Valgimigli M, Orlandi C, Petrou M, Rapezzi C, Stone GW. Long-Term Safety of Drug-Eluting and Bare-Metal Stents. *JACC.* 2015;65:2496–507.
12. Stiehm M, Brede M, Quosdorf D, Martin H, Leder A. A Sensitivity Analysis of Stent Design Parameters using CFD. *Biomed Eng / Biomed Tech.* 2013.

13. Jiménez JM, Davies PF. Hemodynamically Driven Stent Strut Design. *Ann Biomed Eng.* 2009;37:1–24.
14. Duraiswamy N, Schoepfoerster RT, Moore Jr. JE. Comparison of near-wall hemodynamic parameters in stented artery models. *J Biomech Eng.* 2010;131:1–22.
15. Secco GG, Verdoia M, Pistis G, Luca G De, Vercellino M, Parisi R, Reale M, Ballestrero G, Marino PN, Mario C Di. Optical coherence tomography guidance during bioresorbable vascular scaffold implantation. *J Thorac Dis.* 2017;9:986–93.
16. Lipinski MJ, Escarcega RO, Lhermusier T, Waksman R. The Effects of Novel, Bioresorbable Scaffolds on Coronary Vascular Pathophysiology. *J Cardiovasc Transl Res.* 2014;7:413–25.
17. Tenekecioglu E, Sotomi Y, Torii R, Bourantas C V., Miyazaki Y, Collet C, Crake T, Su S, Onuma Y, Serruys PW. Strut protrusion and shape impact on endothelial shear stress: insights from pre-clinical study comparing Mirage and Absorb bioresorbable scaffolds. *Int J Cardiovasc Imaging.* 2017;33:1313–22.
18. Morris PD, Gosling R, Rothman A, Iqbal J, Chiastra C, Colombo M, Migliavacca F, Banning A, Gunn JP. The Double-Kissing Nano-Crush for Bifurcation lesions: Development, Bioengineering, Fluid dynamics and Initial Clinical Testing. *Can J Cardiol.* 2019.
19. Murphy JB, Boyle FJ. A full-range, multi-variable, CFD-based methodology to identify abnormal near-wall hemodynamics in a stented coronary artery. *Biorheology.* 2010;47:117–32.
20. Davies JE, Whinnett ZI, Francis DP, Manisty CH, Aguado-sierra J, Willson K, Foale RA, Malik IS, Hughes AD, Parker KH, Mayet J. Evidence of a Dominant Backward-

- Propagating “ Suction ” Wave Responsible for Diastolic Coronary Filling in Humans, Attenuated in Left Ventricular Hypertrophy. *Circulation*. 2006;113:1768–78.
21. Cho Y, Kensey K. Effects of the non-Newtonian viscosity of blood on flows in a diseased arterial vessel. Part 1: Steady flows. *Biorheology*. 1991;28(3-4):241–62.
 22. Beier S, Ormiston J, Webster M, Cater J, Norris S, Medrano-Gracia P, Young A, Cowan B. Hemodynamics in Idealized Stented Coronary Arteries : Important Stent Design Considerations. *Biomed Eng Soc*. 2016;44:315–29.
 23. Schrauwen JTC, Karanasos A, Ditzhuijzen NS Van, Aben J-P, Van Der Steen AFW, Wentzel JJ, Gijsen FJH. Influence of the Accuracy of Angiography- Based Reconstructions on Velocity and Wall Shear Stress Computations in Coronary Bifurcations : A Phantom Study. *PLoSOne*. 2015;10:1–19.
 24. Malek AM, Alper SL, Izumo S. Hemodynamic Shear Stress and Its Role in Atherosclerosis. *Am Med Assoc*. 1999;282:2035–42.
 25. Ku DN, Giddens DP, Zarins CK, Glagov S. Pulsatile flow and atherosclerosis in the human carotid bifurcation. Positive correlation between plaque location and low oscillating shear stress. *Arteriosclerosis*. 1985;5:293–302.
 26. Zarins CK, Giddens DP, Bharadvaj BK, Sottiurai VS, Mabon RF, Glagov S. Carotid Bifurcation Atherosclerosis. Quantitative Correlation of Plaque Localization with Flow Velocity Profiles and Wall Shear Stress. *Circ Res*. 1983;53:502–14.
 27. Martin D, Boyle F. Sequential Structural and Fluid Dynamics Analysis of Balloon- Expandable Coronary Stents : A Multivariable Statistical Analysis. *Biomed Eng Soc*. 2015;6:314–28.
 28. Thondapu V, Tenekecioglu E, Poon EKW, Collet C, Torii R, Bourantas C V., Chin C,

Disclaimer : As a public service to our readership, this article -- peer reviewed by the Editors of EuroIntervention - has been published immediately upon acceptance as it was received. The content of this article is the sole responsibility of the authors, and not that of the journal

- Sotomi Y, Jonker H, Dijkstra J, Revalor E, Gijssen F, Onuma Y, Ooi A, Barlis P, Serruys PW. Endothelial shear stress 5 years after implantation of a coronary bioresorbable scaffold. *Eur Heart J*. 2018;39:1602–9.
29. Caro CG, Pedley TJ, Schroter RC, Seed WA. Flow in curved pipes. *Mech. Circ.*, 1978, p. 66–8.
30. Roubin GS, Robinson KA, King III SB, Gianturco C, Black AJ, Brown JE, Siegel RJ, Douglas JS. Early and late results of intracoronary arterial stenting after coronary angioplasty in dogs. *Circulation*. 1987;76:891–7.

Figure 1 Scaffold geometry

2-dimensional strut cross-sections (panel 1A). 3-dimensional reconstructed scaffolds (panel 1B).

Figure 2 Blood flow pattern between struts

Streamlines of blood flow between struts in a 2D simulation, with flow direction from left of the image. The recirculation zones distally and proximally to struts are denoted by recirculating vector arrows.

Figure 3 Longitudinal representation of TAWSS in between 2 struts

Struts are denoted by the grey boxes. The x-axis is the normalized position of struts. The y-axis shows the directional TAWSS. The lines represent the TAWSS for each scaffold.

Figure 4 Analysis of strut thickness

The effects of strut thickness on: the size of the recirculation zones proximally and distally to struts, the minimum TAWSS in the recirculation zones and the maximum TAWSS in the recovery zone.

Figure 5 TAWSS and OSI distribution of the different scaffolds

TAWSS (panel A). OSI (panel B). Unwrapped TAWSS distribution map of Fantom Encore (panel C). The scaffold is coloured white. The deployment effects are highlighted in the zoomed cut.

Figure 6 Histograms of the TAWSS and OSI distribution of the scaffolds.

The percentage area with low TAWSS (> 0.5 Pa) and high OSI (> 0.2) is coloured and red and high TAWSS or low OSI is coloured green.

Table 1 Scaffold specifications

Scaffold	Strut Height	Strut Width	Strut Edge Shape	Interstrut Distance	Scaffold Diameter
Fantom Encore	98 μm	150 μm	Rectangular	850 μm	2.5 mm
Fantom	125 μm	150 μm	Rectangular	850 μm	3 mm
Magmaris	150 μm	150 μm	Rounded	~ 1.2 mm	3 mm
Absorb	157 μm	180 μm	Rectangular	1 mm	3 mm

Table 2

Quantification of the effect of each of the scaffold features on TAWSS and OSI in 2D

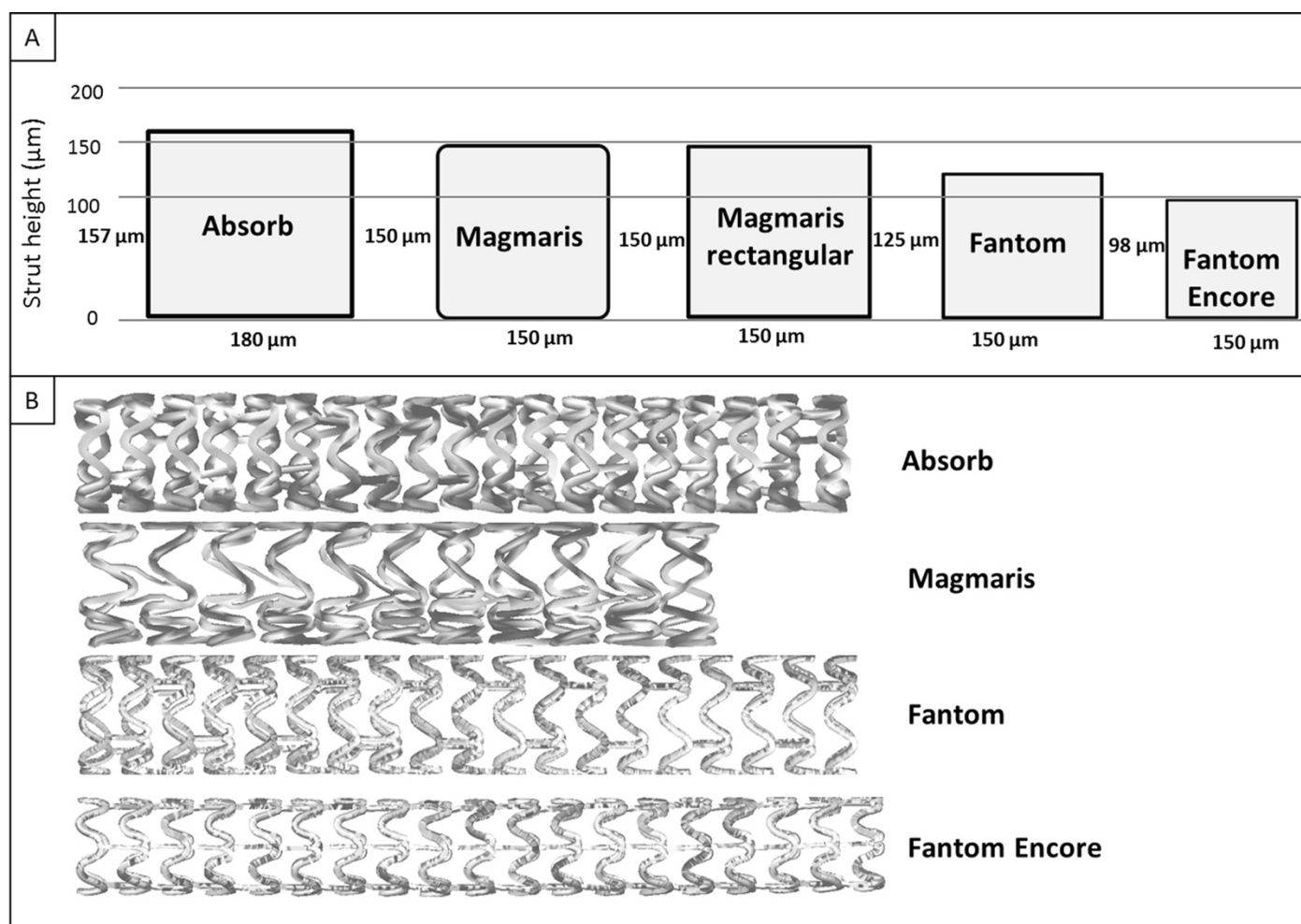
2D simulation	Strut height: -20%	Strut width: -20%	Inter-strut distance: -20%	Strut shape: rounded edges*
Δ recirculation zone**	-37%	0%	0%	-7%
Δ minimum TAWSS	+24%	-5%	+4%	+4%
Δ maximum TAWSS	+28%	-2%	-38%	+7%
Δ maximum OSI	+6%	-5%	+2%	-8%

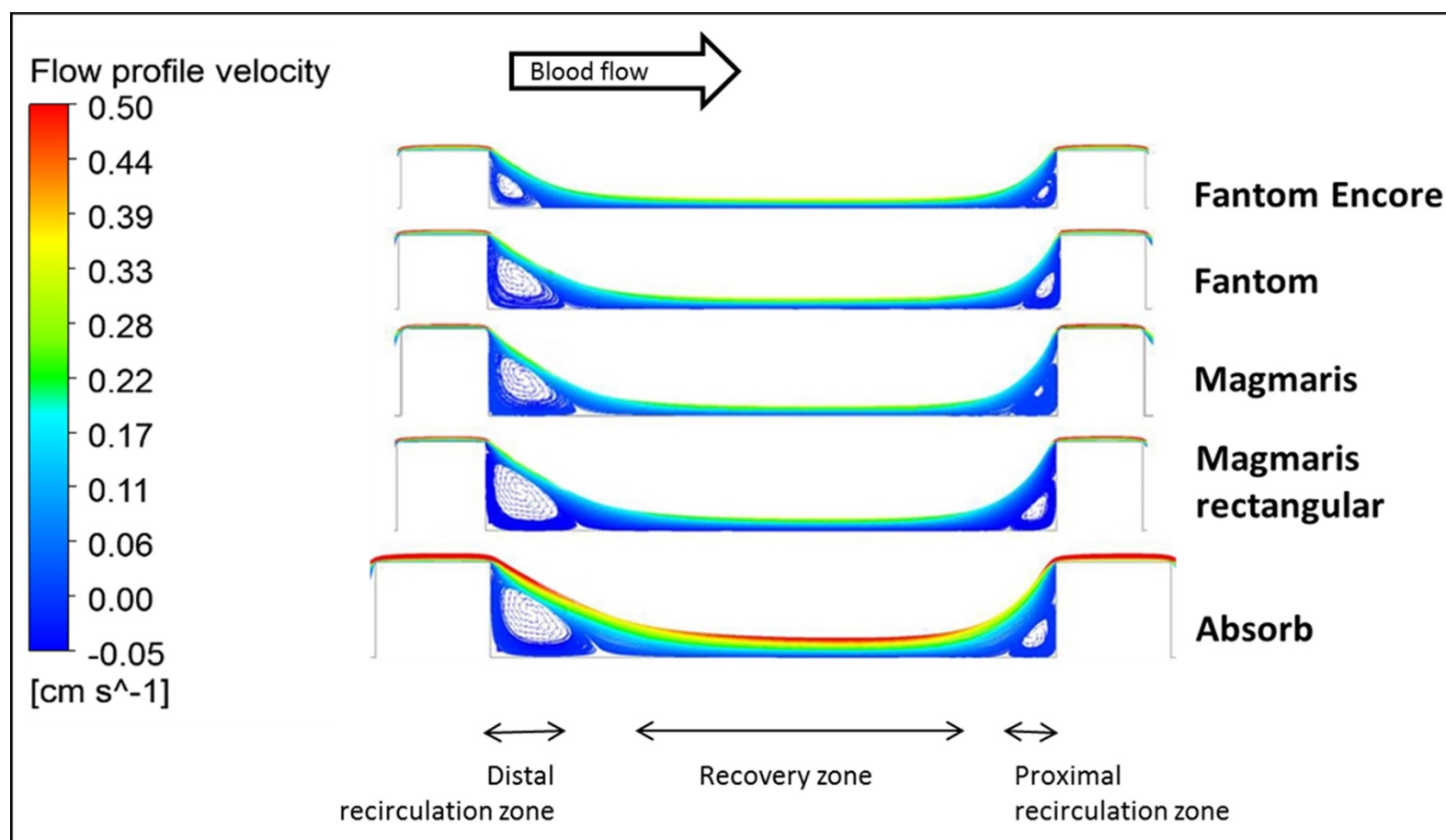
* The hypothetical Magmaris 2D model with rectangular shaped struts is compared to the rounded shaped struts.

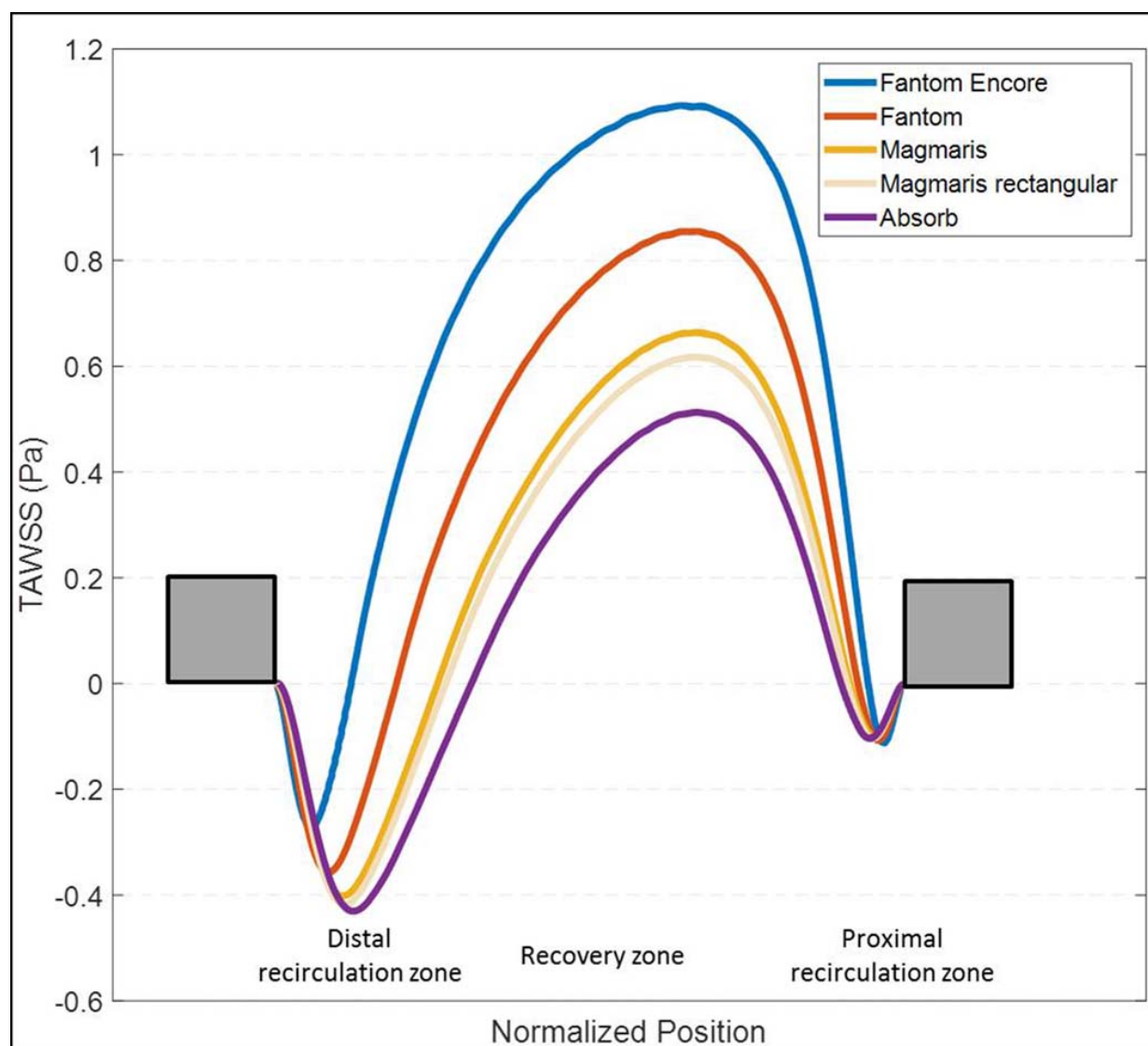
** Distal recirculation zone.

Table 3 TAWSS and OSI distribution specifications

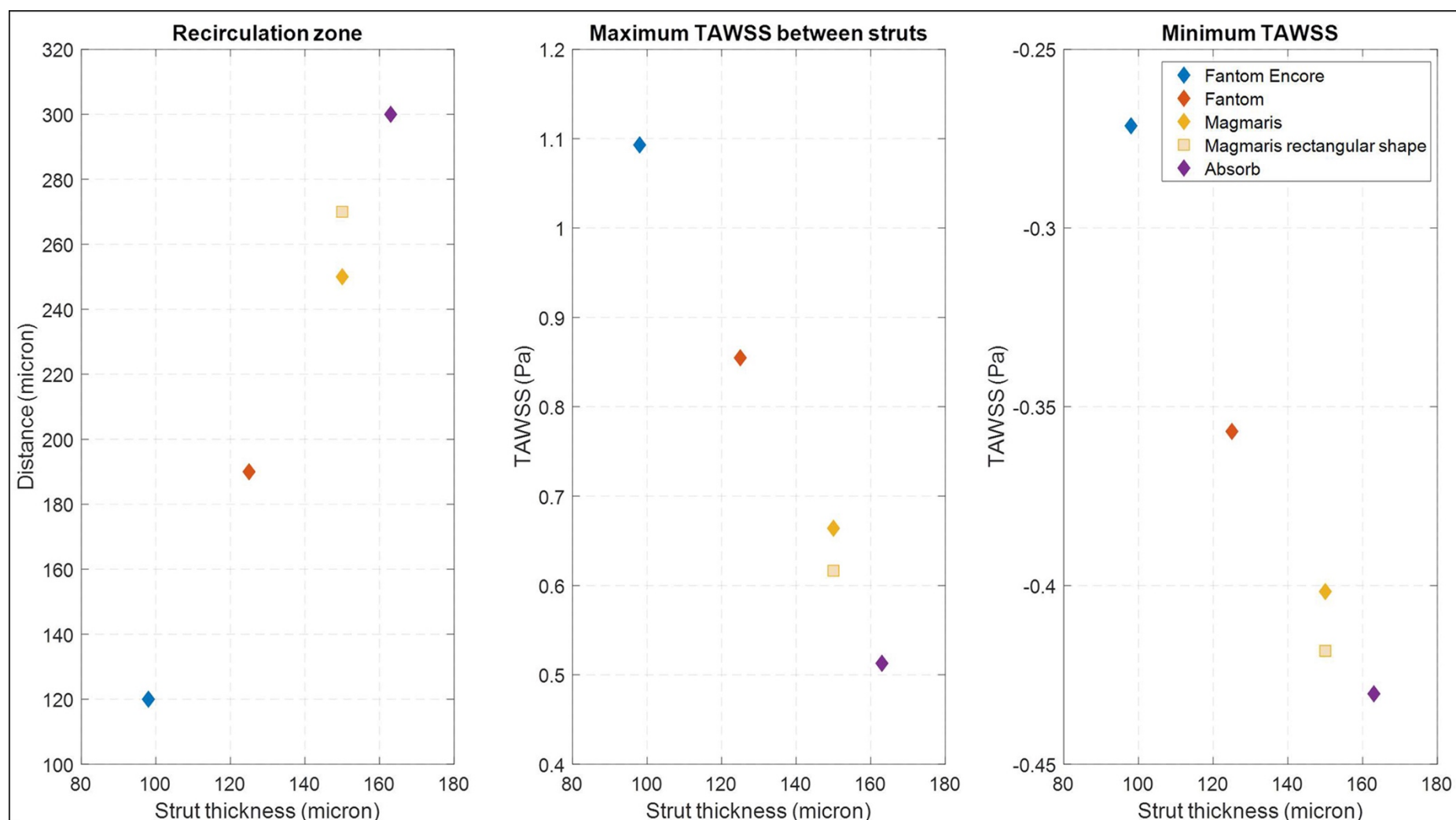
p-value<0.001	TAWSS (Pa)			OSI		
	sd	kurtosis	skewness	sd	kurtosis	skewness
Fantom Encore	0.0054	2.86	1.17	0.012	8.13	1.41
Fantom	0.0059	3.42	1.39	0.011	15.51	2.63
Magmaris	0.0050	3.38	1.35	0.034	11.60	2.66
Absorb	0.0043	5.85	1.99	0.0162	10.02	1.84



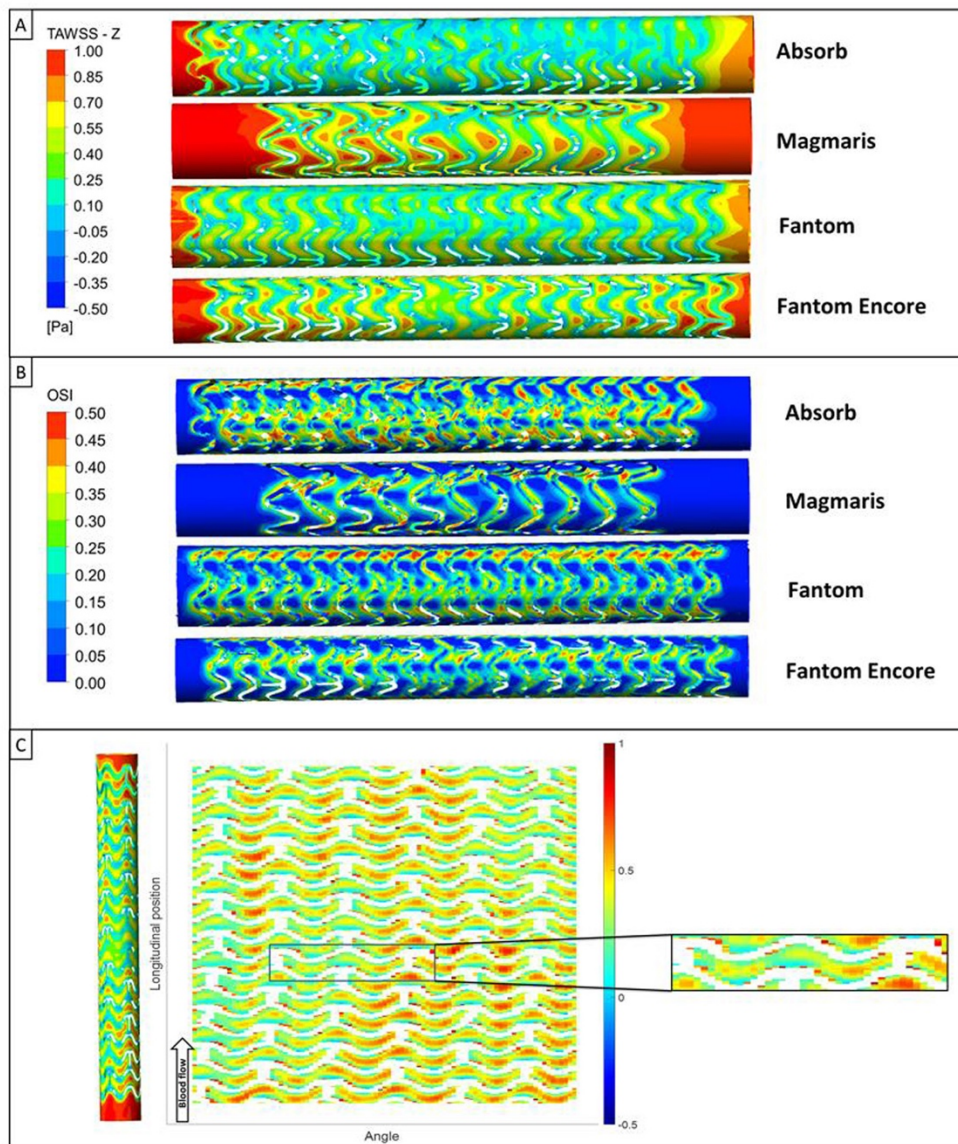




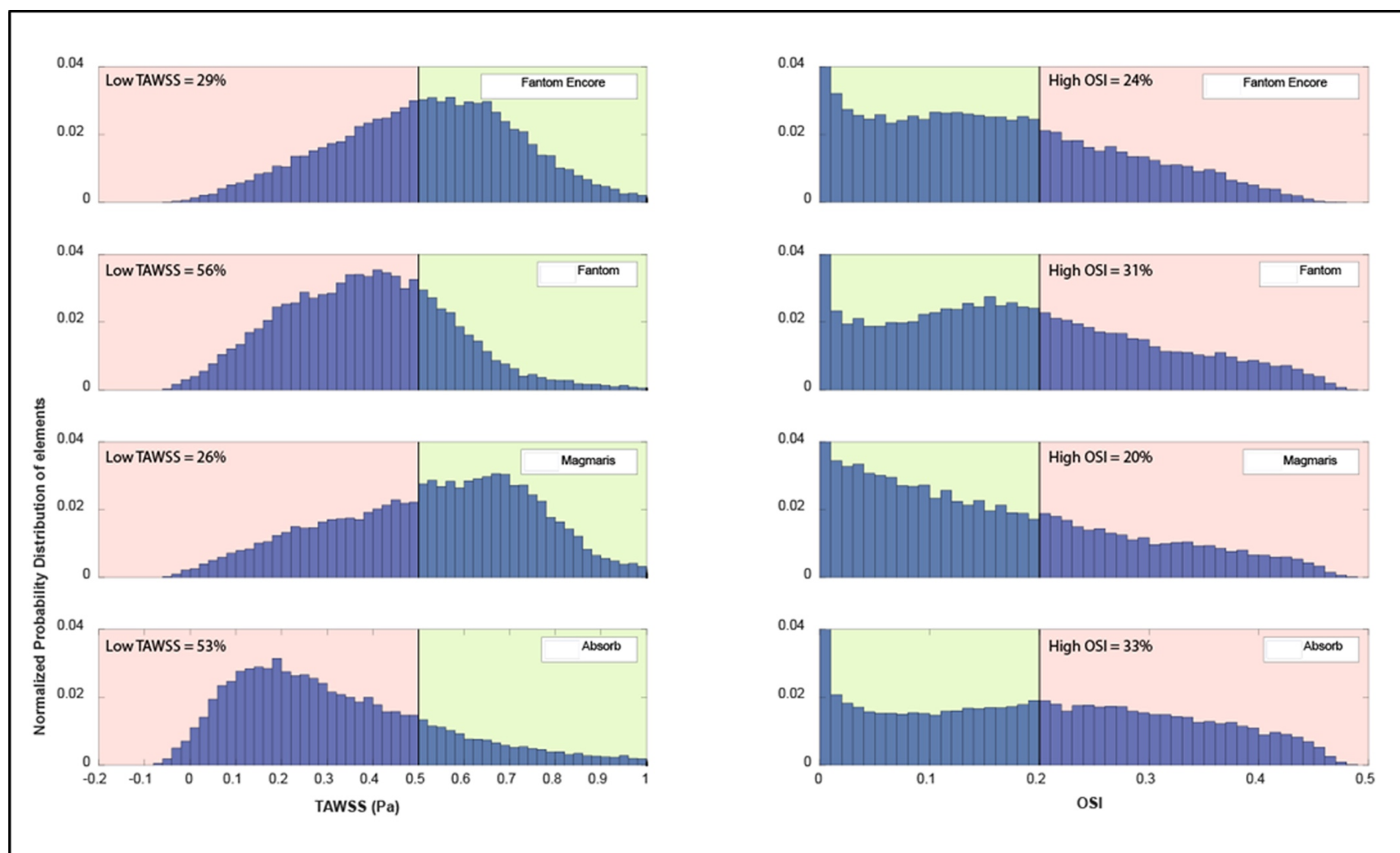
Disclaimer : As a public service to our readership, this article -- peer reviewed by the Editors of EuroIntervention - has been published immediately upon acceptance as it was received. The content of this article is the sole responsibility of the authors, and not that of the journal



Disclaimer : As a public service to our readership, this article -- peer reviewed by the Editors of EuroIntervention - has been published immediately upon acceptance as it was received. The content of this article is the sole responsibility of the authors, and not that of the journal



Disclaimer : As a public service to our readership, this article -- peer reviewed by the Editors of EuroIntervention - has been published immediately upon acceptance as it was received. The content of this article is the sole responsibility of the authors, and not that of the journal



Disclaimer : As a public service to our readership, this article -- peer reviewed by the Editors of EuroIntervention - has been published immediately upon acceptance as it was received. The content of this article is the sole responsibility of the authors, and not that of the journal